KOPIO TN0XX Draft
Beam aspect ratio and FastMC acceptance

David E. Jaffe, BNL

March 7, 2003

Abstract

I compared the signal-to-background (S/B) *vs* signal (S) rates for four different beam aspect ratios ranging from 68×7.3 mrad^2 to 130×3.8 mrad^2. For the Konaka PreRadiator (PR) model, there is no significant difference between the different aspect ratios at the 10% level. For the Zeller PR, the 68×7.3 mrad^2 configuration has a $20 \pm 7\%$ reduction in S/B for the same signal yield compared to the 100×5 mrad^2. The loss appears to be due to degradation of resolution for the 68×7.3 mrad^2 configuration.

1 Introduction

The TDR [1] is based on a beam aspect ratio defined by (horizontal $\times$ vertical) collimation of 100×5 mrad^2. From mechanical considerations of the beam pipe, a narrower and taller beam is desireable. The suppression of neutron halo is less effective with a narrower and taller beam and resolution on reconstructed quantities is expected to be worse due to the less restrictive constraint on the vertical position of the $\mathrm{K^0_L}$.

Jaap Doornbos did a comparison of the neutron halo for four different beam aspect ratios in TechNote TN049 [2]. I used Figure 19 from TN049, reproduced here as Figure 1, to determine the x and y values at Z=1400 cm where the neutron halo was 10^{-4} of the beam. These values are plotted and shown in Figure 3. I corroborated these values with the lower, right hand plot of Figure 20 from TN049 (0.02% contour), reproduced here as Figure 2. An earlier FastMC study [3] found acceptable background levels for neutron halo/beam of 10^{-4}.

Jaap's note assumes an extended target and beam to define beam aspect ratios. The FastMC assumes a point source for $\mathrm{K^0_L}$, so I redefined the beam aspect ratios.

I based my redefinition on $\Theta_x \times \Theta_y = 50 \times 2.5$ as the aspect ratio for the beam used in the TDR and I assume that this aspect ratio corresponds to Jaap's aspect #1. To obtain Θ_y for the FastMC for aspect #2, I scaled by the Jaap's ratios of Θ_y for aspects #1 and #2. Then I set Θ_x such that the solid angle, $\Delta\Omega$, is 500 μSR.

I use the clearances derived from Jaap's results at Z = 1400 cm and the FastMC beam aspect ratios, Table 1, to define the inner aperture at $\mathbf{Z = 1350}$ **cm**, the front of the PR.

	Jaap		FastMC		
	milliradians				μSR
Aspect#	Θ_x	Θ_y	Θ_x	Θ_y	$\Delta\Omega$
1	51	2.6	50	2.5	500
2	42	3.2	40.625	3.077	500.01
3	35	3.8	34.2105	3.654	500.02
4	66	2.0	65	1.923	499.98

Table 1: Comparison of beam aspect ratios used in Jaap's note [2] and in the FastMC for this note. Θ_x and Θ_y are beam half-angles. The total solid angle subtended by the beam is $\Delta\Omega$.

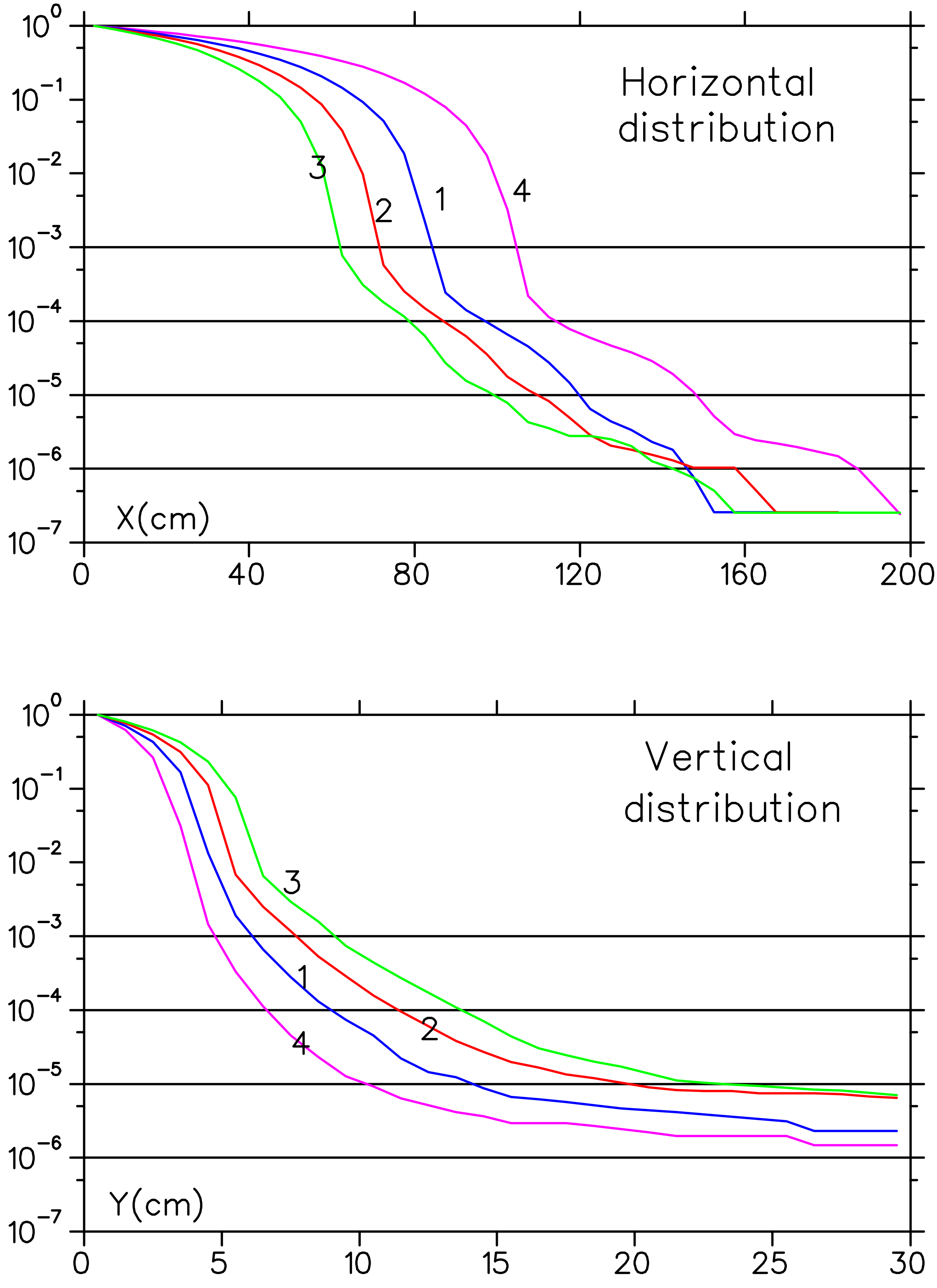

Figure 1: This is Figure 19 of TN049: ' 'Fraction of beam outside the areas, indicated on the horizontal axis."

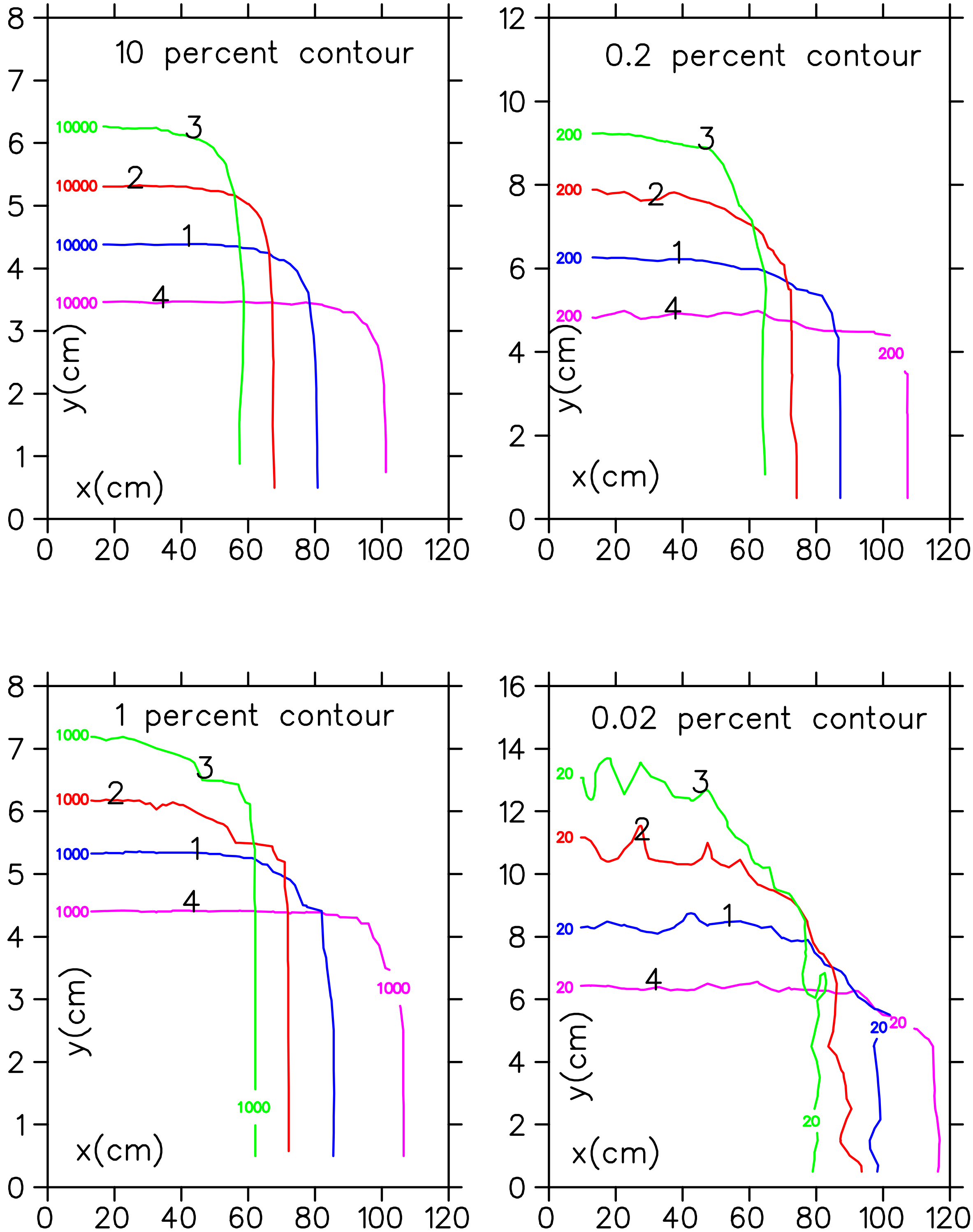

Figure 2: This is Figure 20 of TN049: "Contour plots at 14 m."

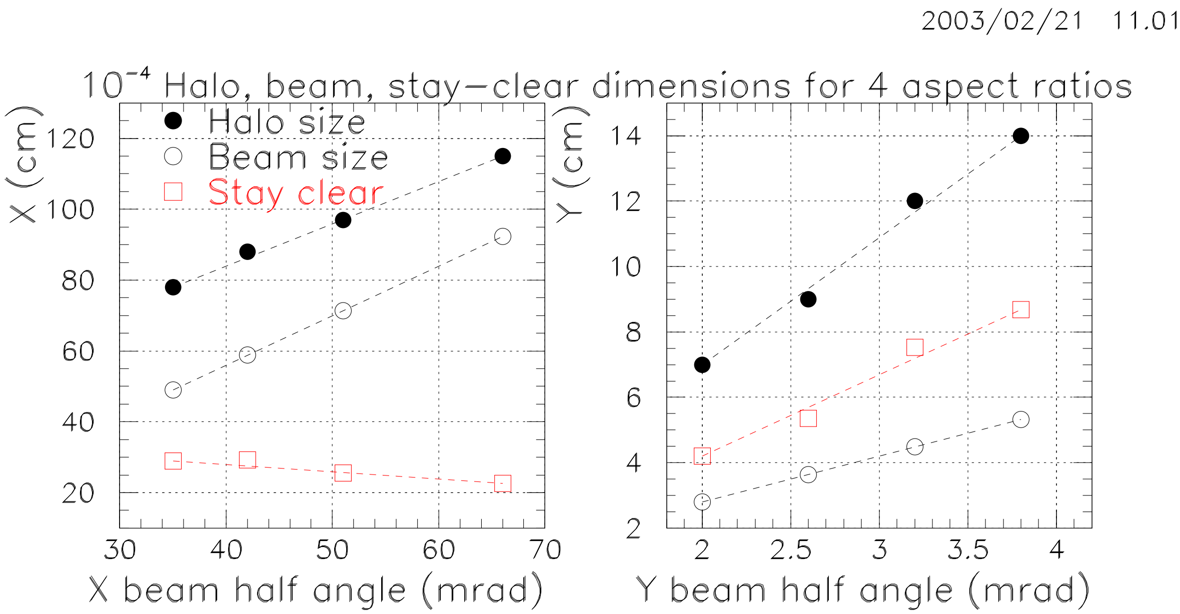

Aspect ratio	ΘX	ΘY	HaloX	HaloY	BeamX	BeamY	ClearX	ClearY	FidSiz
4	66	2	115	7	92.4	2.8	22.6	4.2	19280
3	35	3.8	78	14	49	5.32	29	8.68	18132
2	42	3.2	88	12	58.8	4.48	29.2	7.52	18276
1	51	2.6	97	9	71.4	3.64	25.6	5.36	19008

ΘX,ΘY in mrad, others in cm, FidSiz in cm^2

Figure 3: Definitions of quantities in the figure: Θ_x, Θ_y = beam half angle, BeamX,BeamY = beam half size, HaloX,HaloY = X,Y position where Halo/Beam= 10^{-4}, ClearX,ClearY = clearance = Halo −Beam, FidSiz = fiducial size of PR front face assuming outer limits $150 \times 150 \mathrm{cm}^2$

2 Scope of this study

For the rest of the note, I will refer to aspect ratios in terms of the *full* opening angles instead of the half opening angles.

- I assume a 2.4 second spill with a 2.3 second interspill and a total running time of 12000 hours. The primary proton beam is assumed to be 70 TP/spill. The total number of K^0_L exitting the spoiler is 1.271×10^{16}. The $K^0_L \to \pi^0\nu\bar{\nu}$ branching fraction is taken to be 3×10^{-11}. The K^0_L momentum spectrum is taken from Kapinos [4] for 45°. I assume no production angle dependence of the K^0_L flux across the horizontal aperture.
- This note reports the acceptance for **both** photonss converting in PR. The case of one photon converting in the calorimeter and the other in the PR is not treated.
- The cuts used for comparison were optimized for the 100×5 mrad^2 geometry with clearance 22.5 cm $\times$ 6.625 cm. (For this study, 100×5 mrad^2 has clearance 25.6 cm $\times$ 5.36 cm.)
- There are seven different sets of cuts used to trace a S/B *vs* signal curve. Six of the seven sets were developed with the Konaka PR model. The remaining set of cuts was developed with the Zeller PR model.
- Only backgrounds from major K^0_L decay modes are considered: $3\pi^0$, $2\pi^0$, $\pi^+\pi^-\pi^0$ and $\pi e\nu\gamma$. Non-K^0_L backgrounds and backgrounds from other K^0_L decays were ignored.
- Photons that pass through the beam hole aperture and traverse the PR are included.
- Both Konaka and Zeller PR simulations of the PR were tried.

The Konaka PR model [5] uses an energy-dependent double gaussian to simulate the PR angular resolution. It contains no angular-dependence to the angular resolution.

The Zeller PR model [6] is best described by comments in the code: `A program to reconstruct the response of analog strip pre-radiator for E926. The basic geometry is 2 nested hexagonal tubes with readout between, separated by Pb radiator of thickness TPb (cm). ...Takes average of two analog hits at each plane. Randomize which comes first, x or y. This version has mult scat at each tube.`

For signal events, core resolution on the reconstructed two photon mass $M(\gamma\gamma)$ is significantly worse for Zeller PR and there are larger tails that can be removed with a cut on δ where $\delta \equiv \sqrt{\delta_x^2 + \delta_y^2}$ where δ_x, δ_y is the difference in x,y between measured e^- and e^+ positions at last plane used for measurement. There is no equivalent quantity available from the Konaka PR model. The effect of an energy-dependent cut on δ on $M(\gamma\gamma)$ is shown in Figure 4 after the application of the basic cuts. The **basic cuts** are

1. SKIM CUTS: defined below.
2. FitOK: no singular matrix encountered in the fit,

3. EK: $638 < E(K) < 1486$ MeV where $E(K)$ is the reconstructed candidate K_L^0 energy,

4. ZK: $1025 < Z(K) < 1300$ cm where $Z(K)$ is the Z position of the reconstructed candidate K_L^0,

5. dif: $\delta < max(1., 4.-0.005*E_\gamma(MeV))$ cm, where δ is defined above and $E_\gamma(MeV)$ is the fitted photon energy.

The definition of the SKIM CUTS:

- Generated Photon at 10 radiation lengths into PR/CAL $|X| < 300.00, |Y| < 300.00$ cm

- For the reconstructed K_L^0 candidate:
  - $0.00 < E(K) < 1486.00$ MeV and
  - $0.00 < Z(K) < 2000.00$ cm

- For the reconstructed π^0 candidate:
  - $0.00 < E^*(\pi) < 240.00$ MeV
  - $100.00 < M(\gamma\gamma) < 170.00$ MeV/c^2
  - $E^*(\pi) - |E^*(\gamma 1) - E^*(\gamma 2)| > 0.0$ MeV

The SKIM CUTS have been applied for all results presented in this note. The **basic cuts** were applied for resolution and bias studies in the next section.

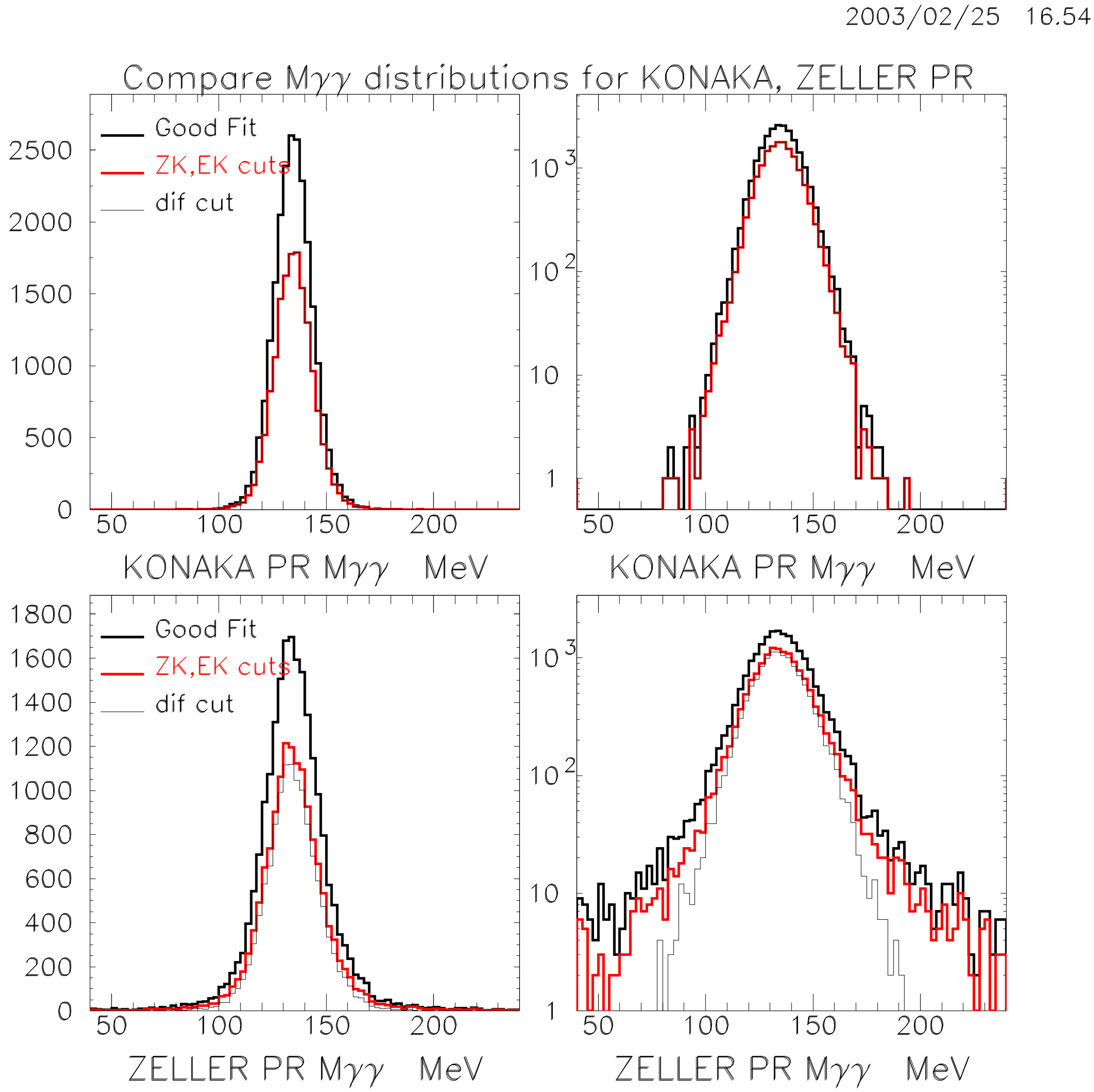

Figure 4: Comparison of $M(\gamma\gamma)$ distributions for the Konaka and Zeller PR models after successive application of basic cuts.

3 Comparison of resolution and bias

I did extensive comparison of the core resolution and the bias of reconstructed and fitted quantities determined by the FastMC. The core resolution is defined as the σ of a gaussian fit to a distribution where the fit is restricted to $\pm 2\sigma$ about the fitted mean (multiple iterations are done for each gaussian fit to obtain a stable value of σ and the mean). The bias is simply the fitted mean of the distribution of the difference of the measured and generated value of a quantity.

The **basic cuts** were applied for the resolution and bias studies.

Figures 5, 6, 7, 8 and 9 show the core resolution on $M(\gamma\gamma)$, $P^*(\pi^0)$, $Z(K)$, $E(\gamma)$ and $E^*(\gamma)$, respectively, as a function of $Z(K)$, $|\Theta_X|$, $|\Theta_Y|$, $E(\gamma)$, $E^*(\gamma)$, $|A_X|$ or $|A_Y|$. $P^*(\pi^0)$ is the magnitude of the momentum of the π^0 in the K^0_L CMS, $|\Theta_{X(Y)}|$ is the magnitude of the production angle in X(Y) of the K^0_L, $E(\gamma)$ is the photon energy in the lab, $E^*(\gamma)$ is the photon energy in the K^0_L CMS, and $|A_{X(Y)}|$ is the magnitude of the production angle in X(Y) of the photon. Figures 10, 11, 12, 13 and 14 show the bias on $M(\gamma\gamma)$, $P^*(\pi^0)$, $Z(K)$, $E(\gamma)$ and $E^*(\gamma)$, respectively.

Figure 5 shows that the $M(\gamma\gamma)$ resolution is significantly worse for the Zeller PR model and that there is a stronger dependence of the resolution on $Z(K)$ than the Konaka PR model. In addition, there is a clear degradation of $M(\gamma\gamma)$ resolution as the K^0_L vertical production angle increases for both models, although the effect is more evident for the Zeller PR model. (This is contrary to previous statements I made that were based on lower statistics.) The overall signal efficiency with the Zeller PR model is $\sim 75\%$ of the signal efficiency with the Konaka PR model mainly due to the the poorer $M(\gamma\gamma)$ resolution.

Figure 6 shows that $P^*(\pi^0)$ resolution degrades with increasing $Z(K)$ in the same manner as $M(\gamma\gamma)$. In addition, the $P^*(\pi^0)$ resolution for the 68×7.3 mrad^2 configuration is about 0.5 MeV/c worse compared to 100×5 mrad^2 for all values of $Z(K)$. The degradation of $P^*(\pi^0)$ resolution as a function of Θ_Y is evident for both models.

Figure 7 shows that the $Z(K)$ resolution improves from ~ 10.5 cm to $\sim 3.5 cm$ from the upstream to the downstream end of the fiducial volume for the Zeller PR model, independent of the beam aspect ratio. The $Z(K)$ resolution for Konaka PR model is about 1 cm worse than that of the Zeller PR model.

The lab photon energy resolution improves with $Z(K)$ as shown in Figure 8 independent of the beam aspect ratio. The improvement is relative greater with the Konaka PR model.

Figure 9 shows a stronger dependence of the $E^*(\gamma)$ resolution on $Z(K)$ with the Zeller PR model than the Konaka PR model. There is also a clear degradation in $E^*(\gamma)$ resolution as the K^0_L vertical production angle increases for both models.

The bias on $M(\gamma\gamma)$ in Figure 10 is ~ 0.5 MeV with both PR models and independent of $Z(K)$ and the K^0_L production angle.

There is a slight dependence of the $P^*(\pi^0)$ bias on $Z(K)$ as shown in Figure 11. More importantly, the bias with the Zeller PR model as ~ 0.5 MeV/c greater than with the Konaka PR model. Thus cuts on $P^*(\pi^0)$ designed with the Konaka PR model may be less effective when applied to the the Zeller PR model. Lower and upper limits are set on $P^*(\pi^0)$ to exclude $\mathrm{K}^0_\mathrm{L} \to 3\pi$ and $\mathrm{K}^0_\mathrm{L} \to \pi^0\pi^0$, respectively, so a different bias will allow differing amounts of these backgrounds.

There is a relatively strong bias on $Z(K)$ for decays in the most upstream part of the fiducial volume as shown in Figure 12 and the bias with the Konaka PR model is

~ 1 cm greater than the Zeller PR model independent of $Z(K)$.

The bias on the lab photon energy decreases(increases) with $Z(K)(E(\gamma))$ as shown in Figure 13 independent of beam aspect ratio. There is a strong dependence on $E^*(\gamma)$ of the bias in $E^*(\gamma)$ as shown in Figure 14.

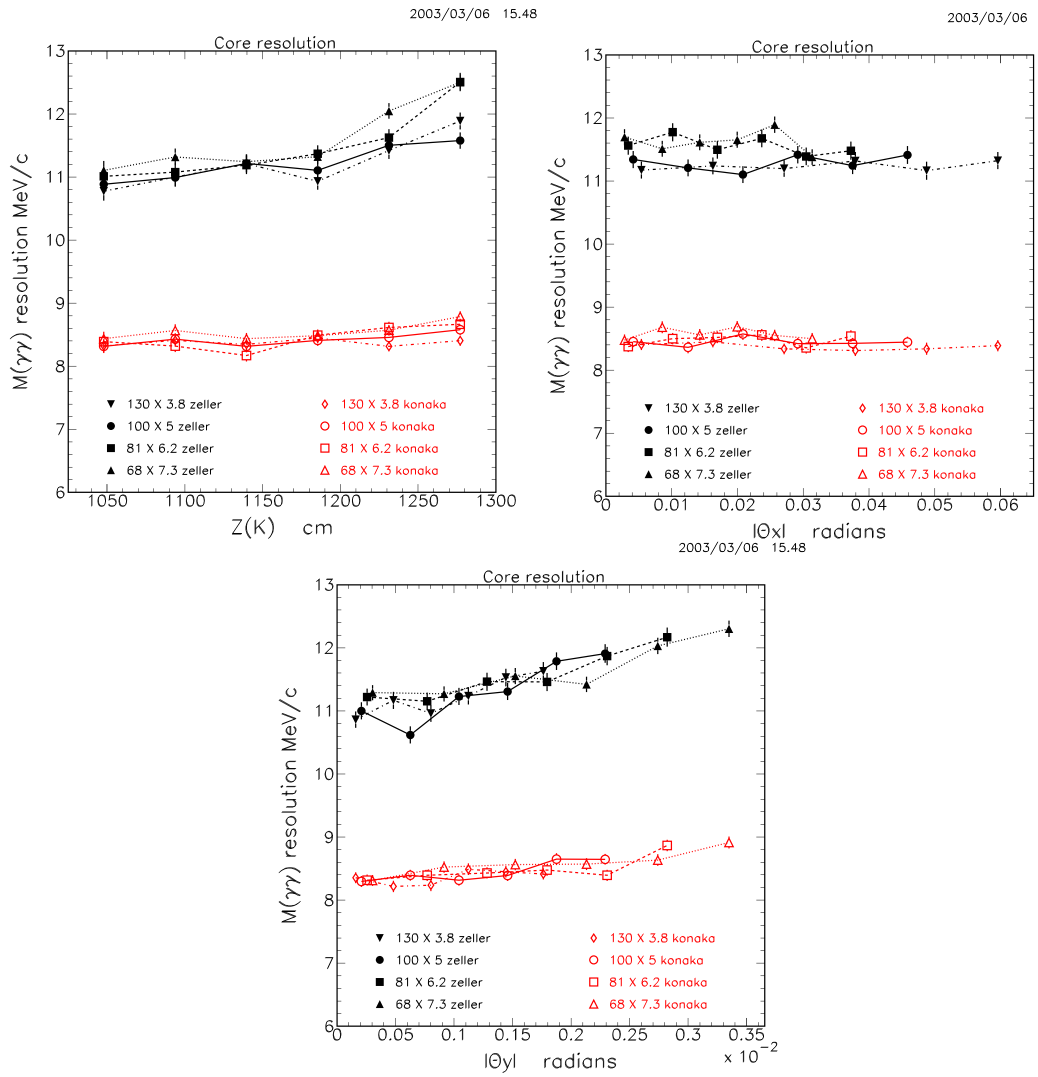

Figure 5: $M(\gamma\gamma)$ core resolution as a function of $Z(K)$, $|\Theta_X|$ and $|\Theta_Y|$ for the Konaka and Zeller PR models for the four different beam aspect ratios after application of basic cuts.

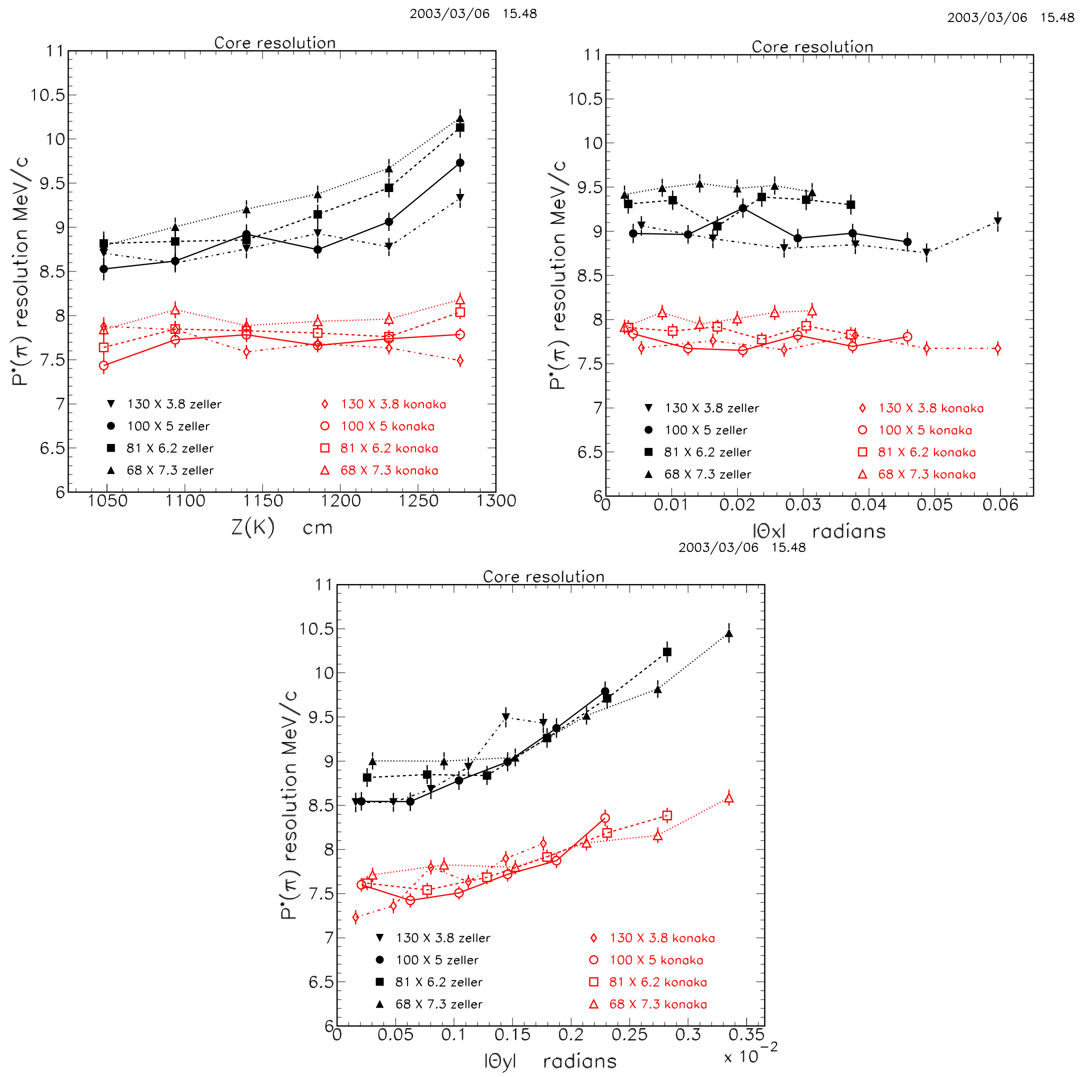

Figure 6: $P^{*}(\pi^{0})$ core resolution as a function of $Z(K)$, $|\Theta_X|$ and $|\Theta_Y|$ for the Konaka and Zeller PR models for the four different beam aspect ratios after application of basic cuts.

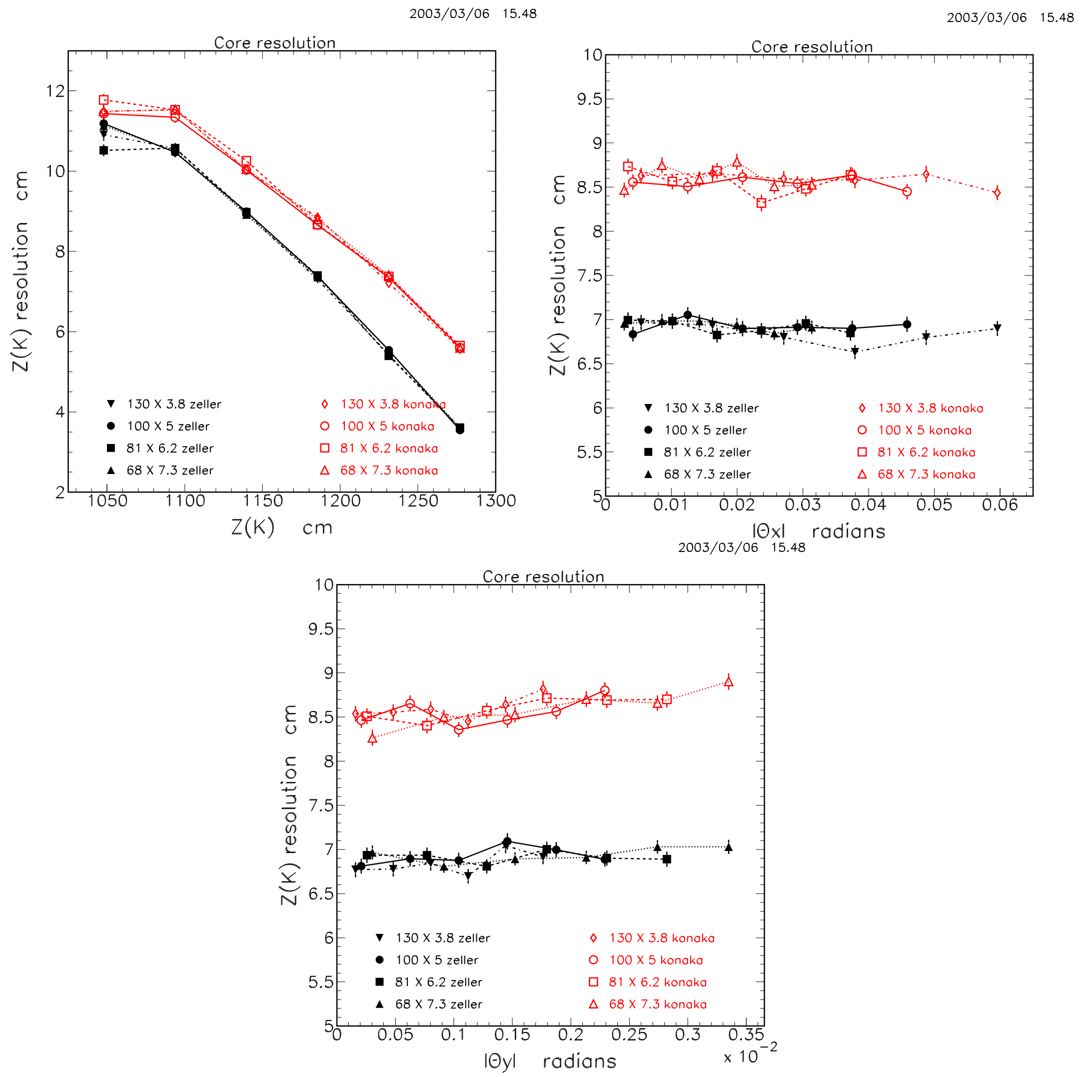

Figure 7: $Z(K)$ core resolution as a function of $Z(K)$, $|\Theta_X|$ and $|\Theta_Y|$ for the Konaka and Zeller PR models for the four different beam aspect ratios after application of basic cuts.

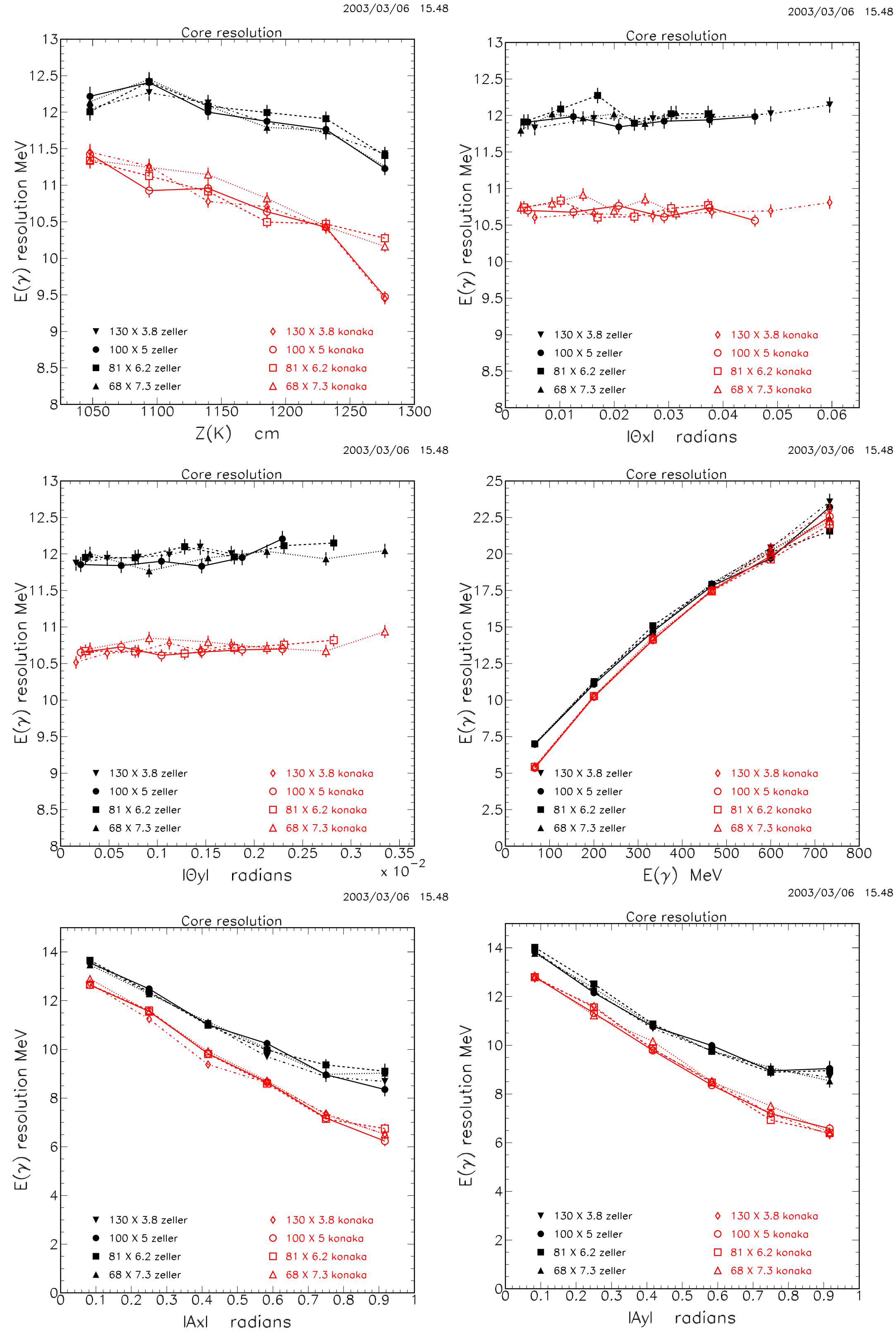

Figure 8: $E(\gamma)$ core resolution as a function of $Z(K)$, $|\Theta_X|$, $|\Theta_Y|$, $E(\gamma)$, $|A_X|$ and $|A_Y|$ for the Konaka and Zeller PR models for the four different beam aspect ratios after application of basic cuts.

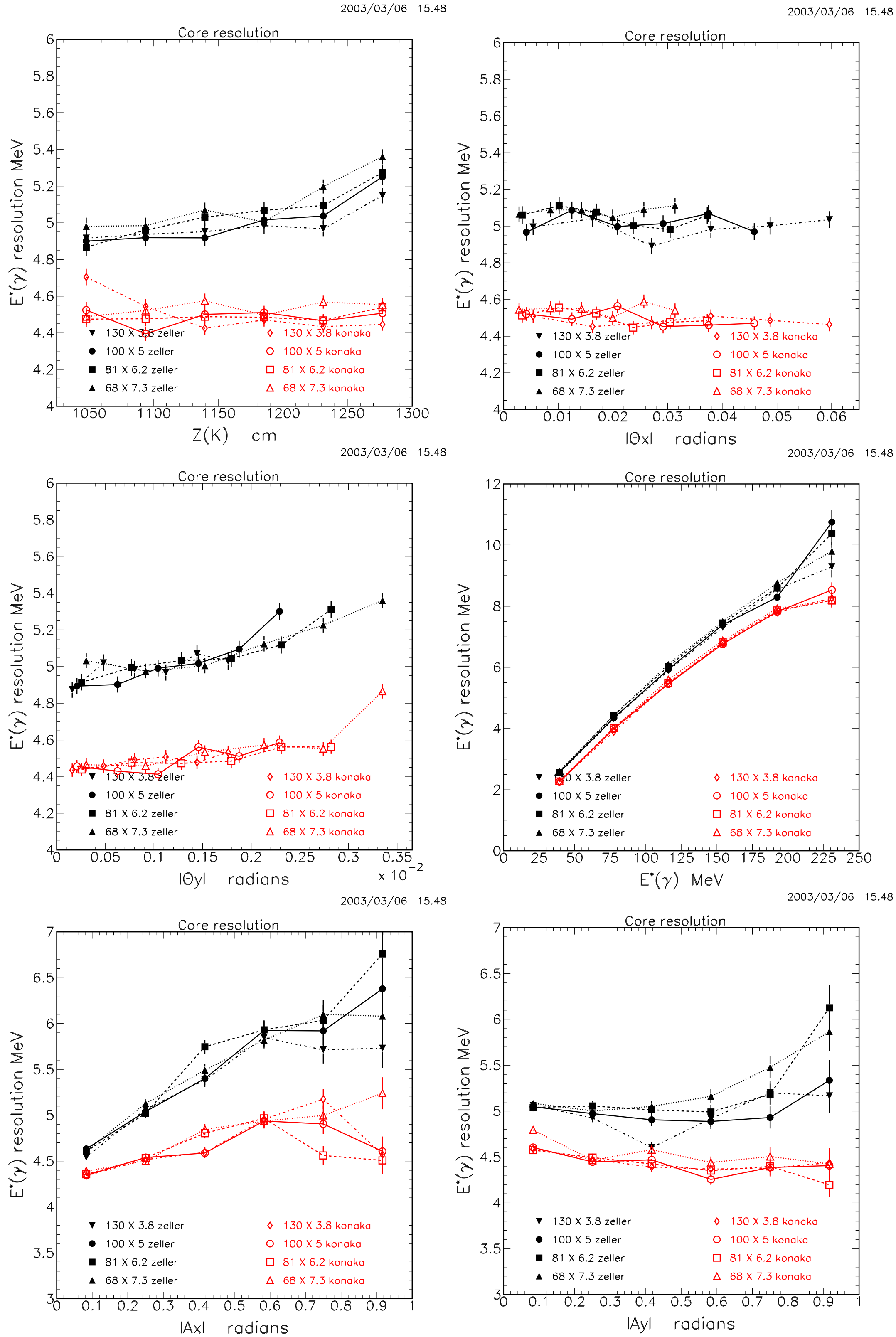

Figure 9: $E^*(\gamma)$ core resolution as a function of $Z(K)$, $|\Theta_X|$, $|\Theta_Y|$, $E^*(\gamma)$, $|A_X|$ and $|A_Y|$ for the Konaka and Zeller PR models for the four different beam aspect ratios after application of basic cuts.

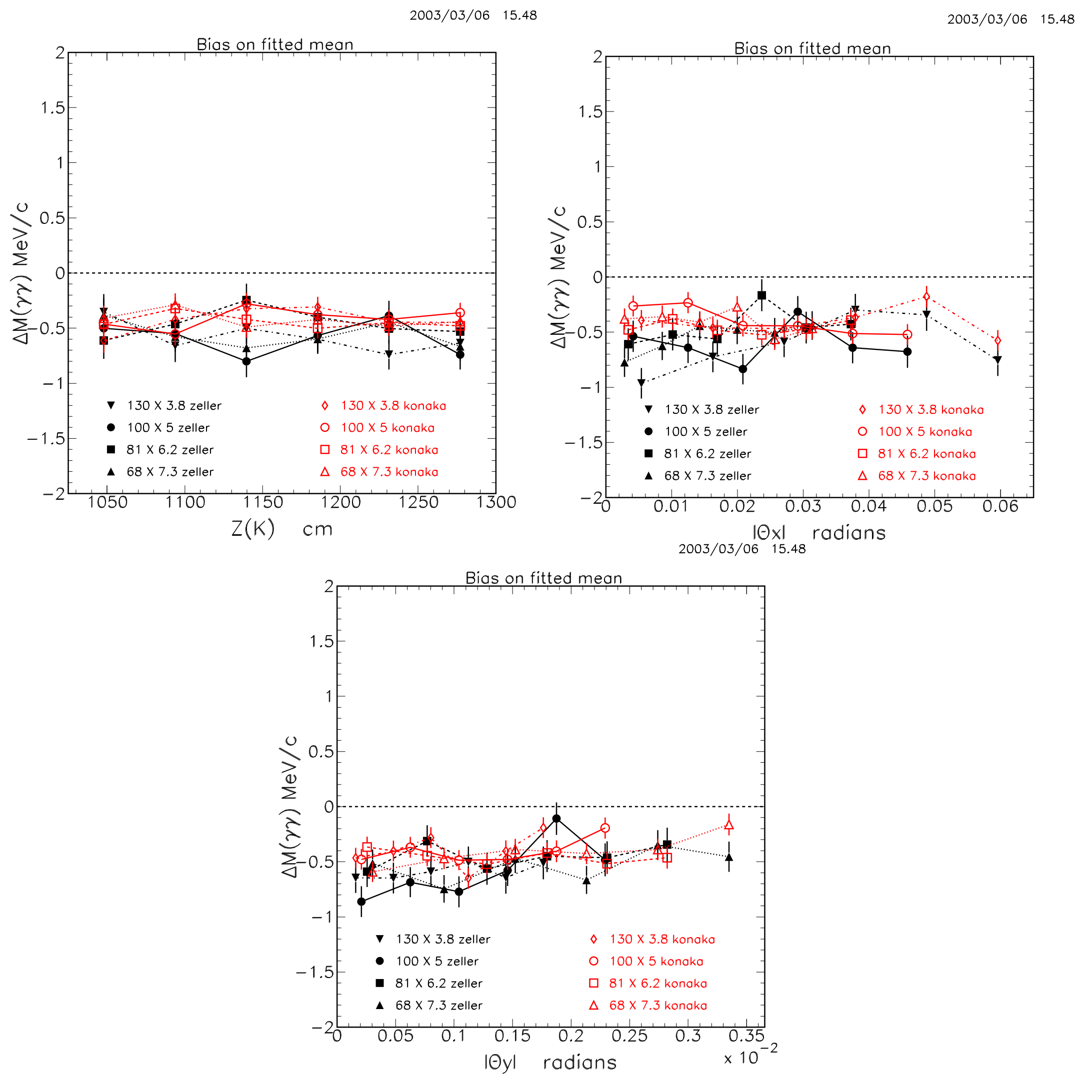

Figure 10: $M(\gamma\gamma)$ bias as a function of $Z(K)$, $|\Theta_X|$ and $|\Theta_Y|$ for the Konaka and Zeller PR models for the four different beam aspect ratios after application of basic cuts.

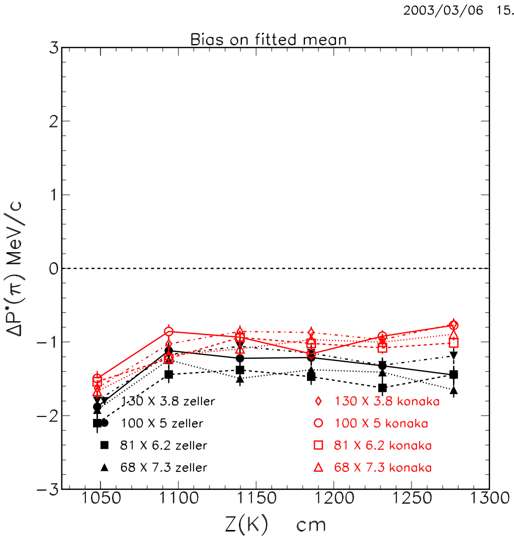

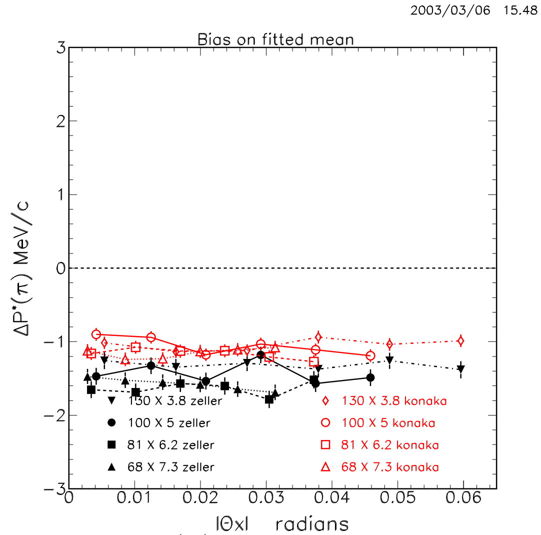

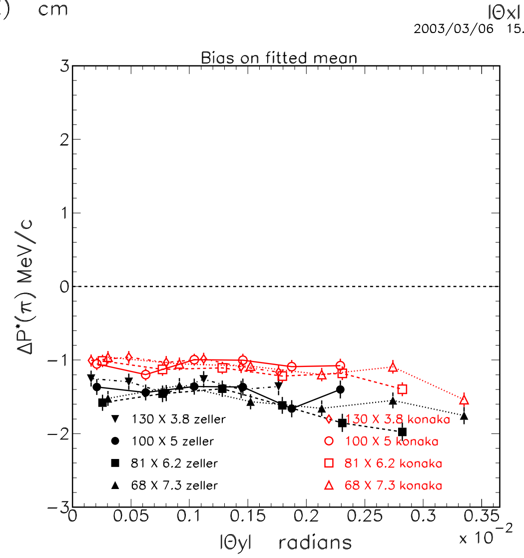

Figure 11: $P^*(\pi^0)$ bias as a function of $Z(K)$, $|\Theta_X|$ and $|\Theta_Y|$ for the Konaka and Zeller PR models for the four different beam aspect ratios after application of basic cuts.

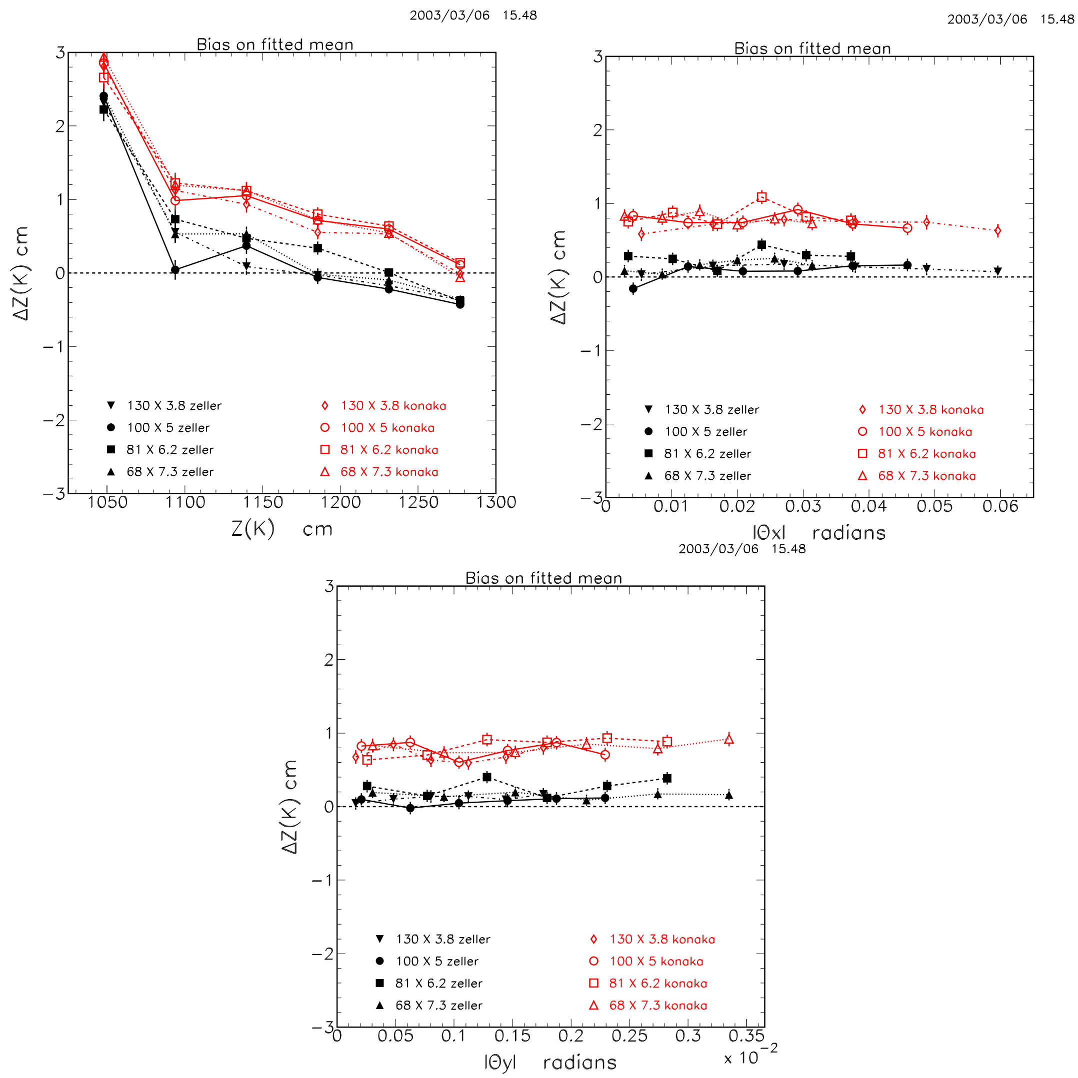

Figure 12: $Z(K)$ bias as a function of $Z(K)$, $|\Theta_X|$ and $|\Theta_Y|$ for the Konaka and Zeller PR models for the four different beam aspect ratios after application of basic cuts.

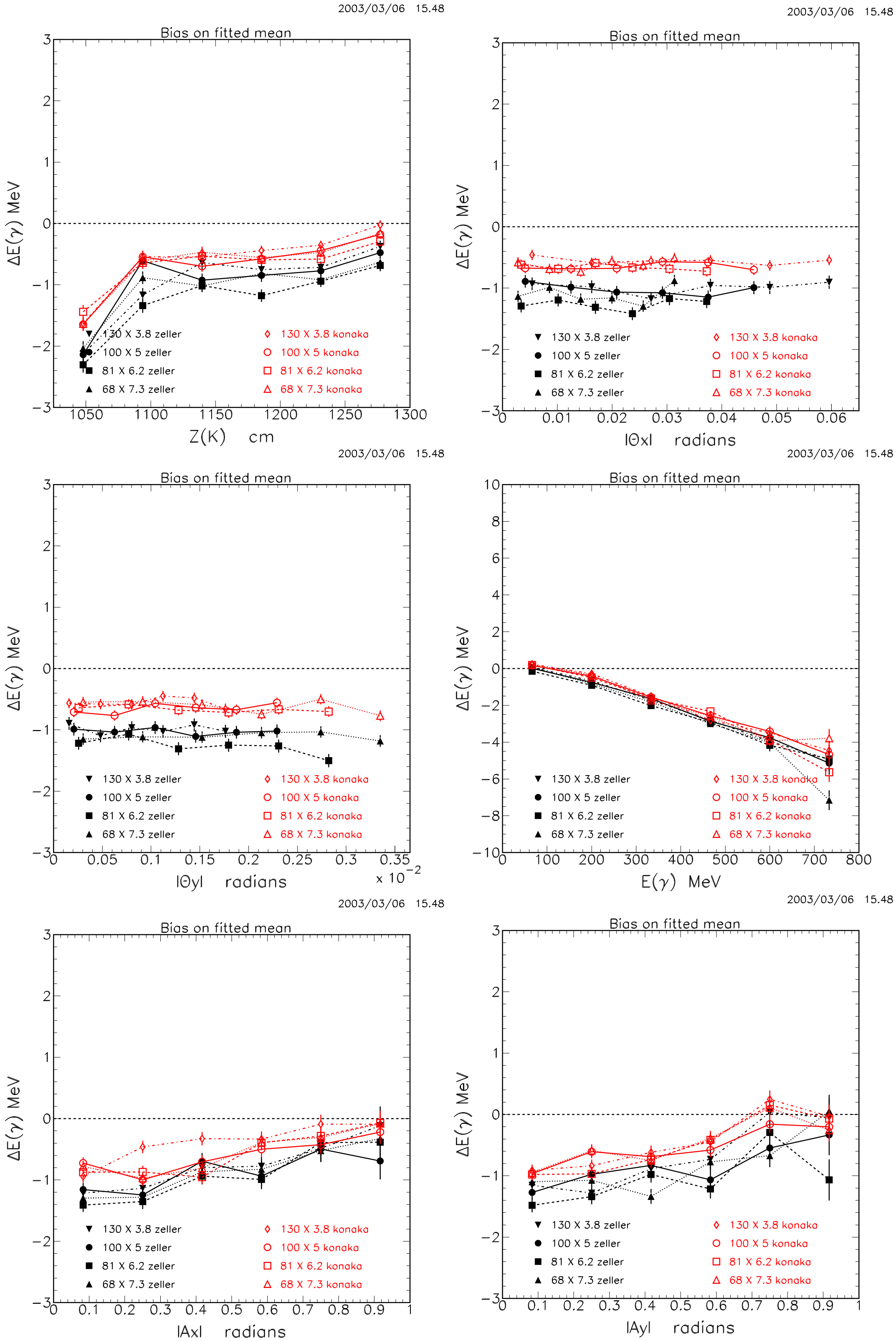

Figure 13: $E(\gamma)$ bias as a function of $Z(K)$, $|\Theta_X|$, $|\Theta_Y|$, $E(\gamma)$, $|A_X|$ and $|A_Y|$ for the Konaka and Zeller PR models for the four different beam aspect ratios after application of basic cuts.

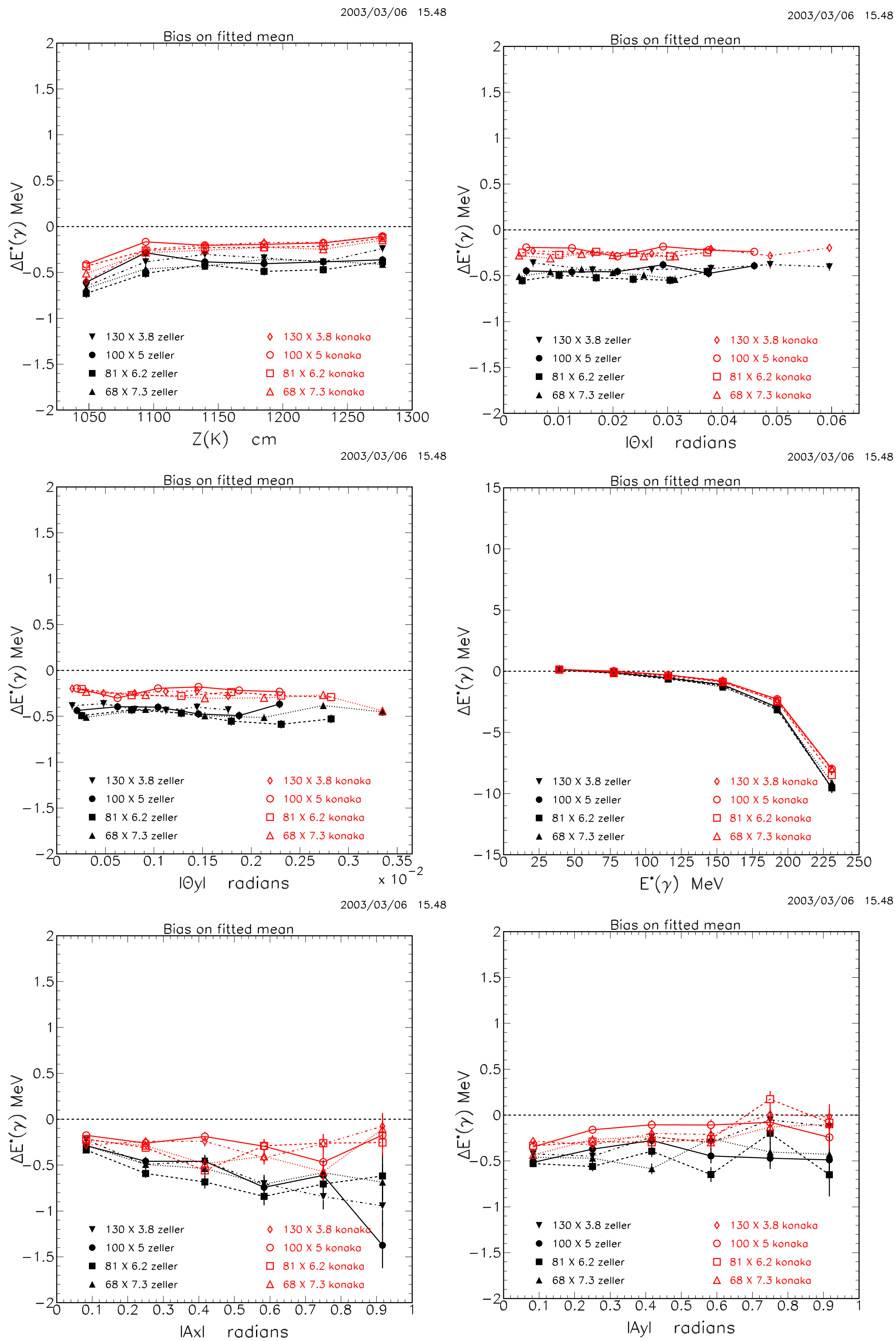

Figure 14: $E^*(\gamma)$ bias as a function of $Z(K)$, $|\Theta_X|$, $|\Theta_Y|$, $E^*(\gamma)$, $|A_X|$ and $|A_Y|$ for the Konaka and Zeller PR models for the four different beam aspect ratios after application of basic cuts.

4 Acceptance

Figures 15 and 16 show S/B *vs* signal for the four different beam aspect ratios. The calculated signal rate with the Zeller PR model is $\sim 75\%$ of that with the Konaka PR model as described in Section 2. At the $\sim 10\%$ level of statistical precision, there is no significant difference in the S/B *vs* signal curves for the four different aspect ratios with the Konaka PR model as seen in Figure 16. However, there is a significant loss of acceptance between the two narrower and taller aspect ratios and the wider and shorter aspect ratios with the Zeller PR model as seen in Figure 15. The size of the FastMC sample for the 68×7.3 mrad^2 configuration with the Zeller PR model is four times larger than the samples for the other configurations in order to confirm the magnitude of the loss.

The ratio of S/B for the 81×6.1 mrad^2, 68×7.3 mrad^2 and 130×3.8 mrad^2 configurations to the S/B for the 100×5 mrad^2 configuration as a function of the expected signal yield with the Zeller PR model is shown in Figure 17. The value of S/B and its uncertainty for each configuration at each value of signal yield was estimated from the results shown in Figures 15 and 16 by interpolation. The central plot in Figure 17 clearly shows a drop in S/B of $20 \pm 7\%$ or more for signal yields of 50 events or more. There is a drop in S/B for yields of less than 50 events although with less statistical precision. The degradation in the $M(\gamma\gamma)$ and $P^*(\pi^0)$ resolution with larger $\mathrm{K^0_L}$ vertical production angles is the most likely explanation of the drop in acceptance.

A similar comparison with the Konaka PR model in Figure 18 confirms the consistency of the yields for the different aspect ratios.

5 Conclusion

Narrower and taller beam aspect ratios with respect to the 100×5 mrad^2 configuration used in the TDR have significantly lower acceptance ($20 \pm 7\%$) with the Zeller PR model due to the degradation in $M(\gamma\gamma)$ and $P^*(\pi^0)$ resolution. The degradation in resolution for these quantities is less severe with the Konaka PR model and no significant difference in acceptance is seen between aspect ratios ranging from 68×7.3 mrad^2 to 130×3.8 mrad^2.

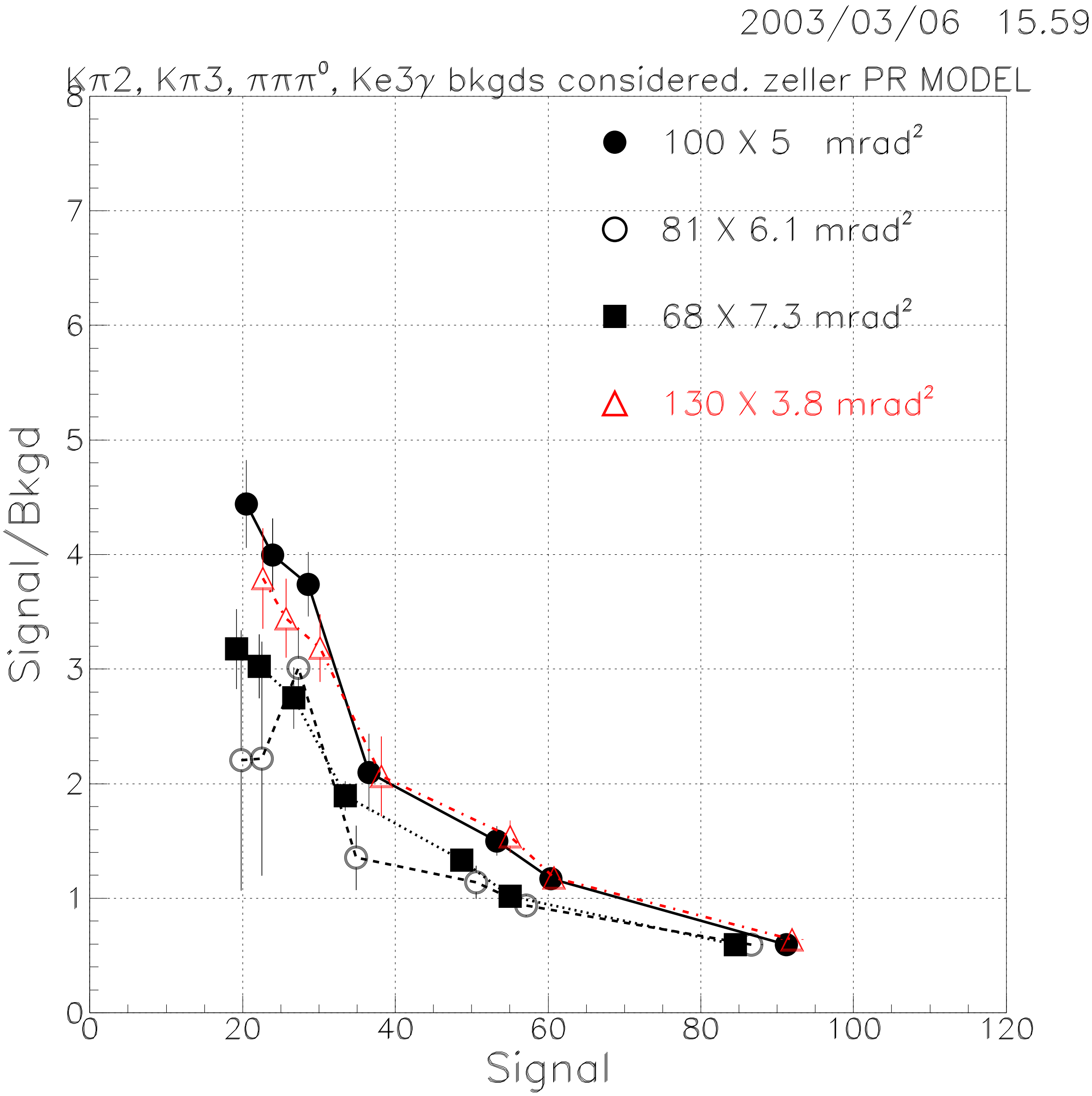

Figure 15: Signal/Background *vs* signal for the four different beam aspect ratios shown with the Zeller PR model. The uncertainties are statistical only.

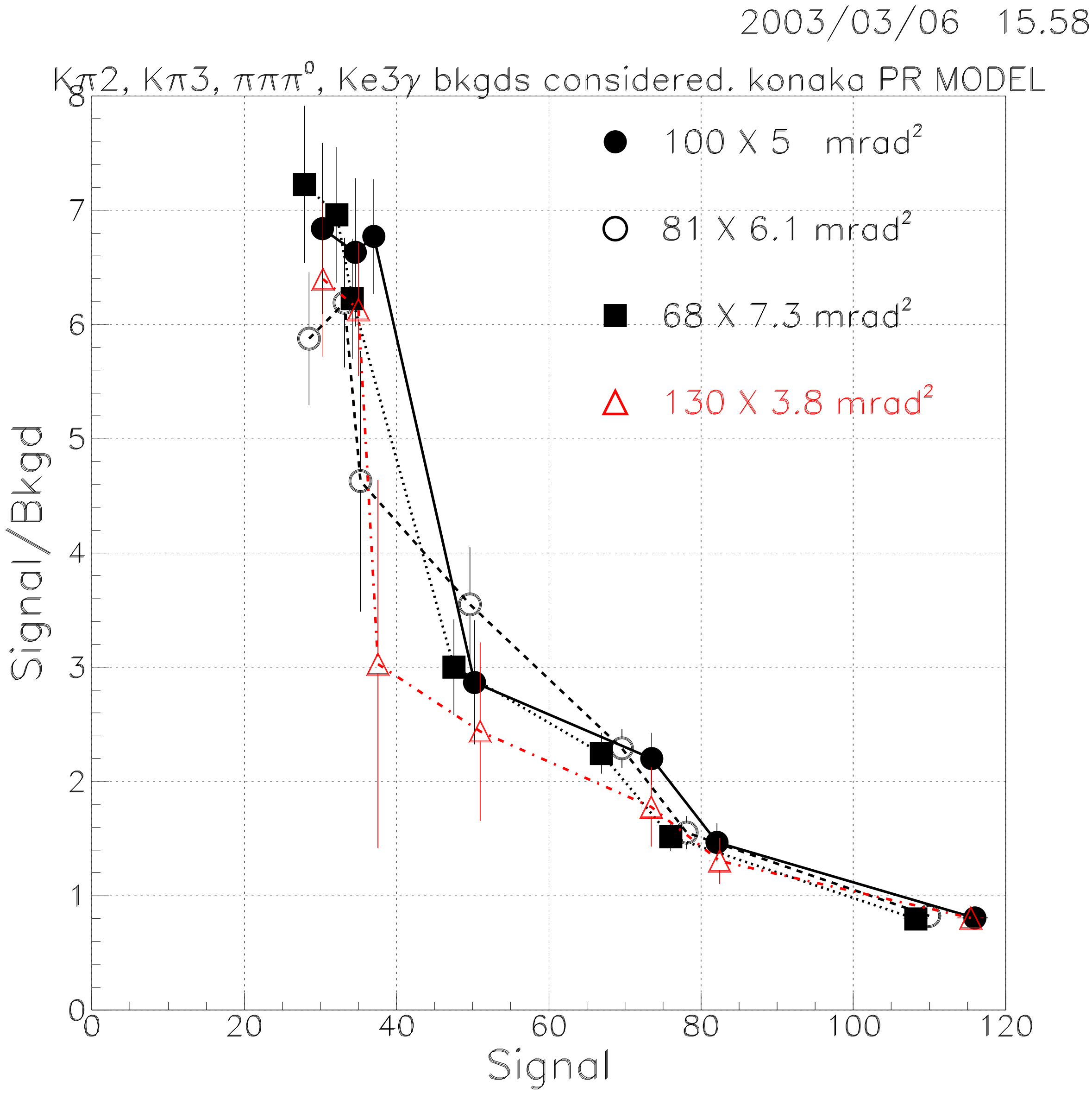

Figure 16: Signal/Background *vs* signal for the four different beam aspect ratios shown with the Konaka PR model. The uncertainties are statistical only.

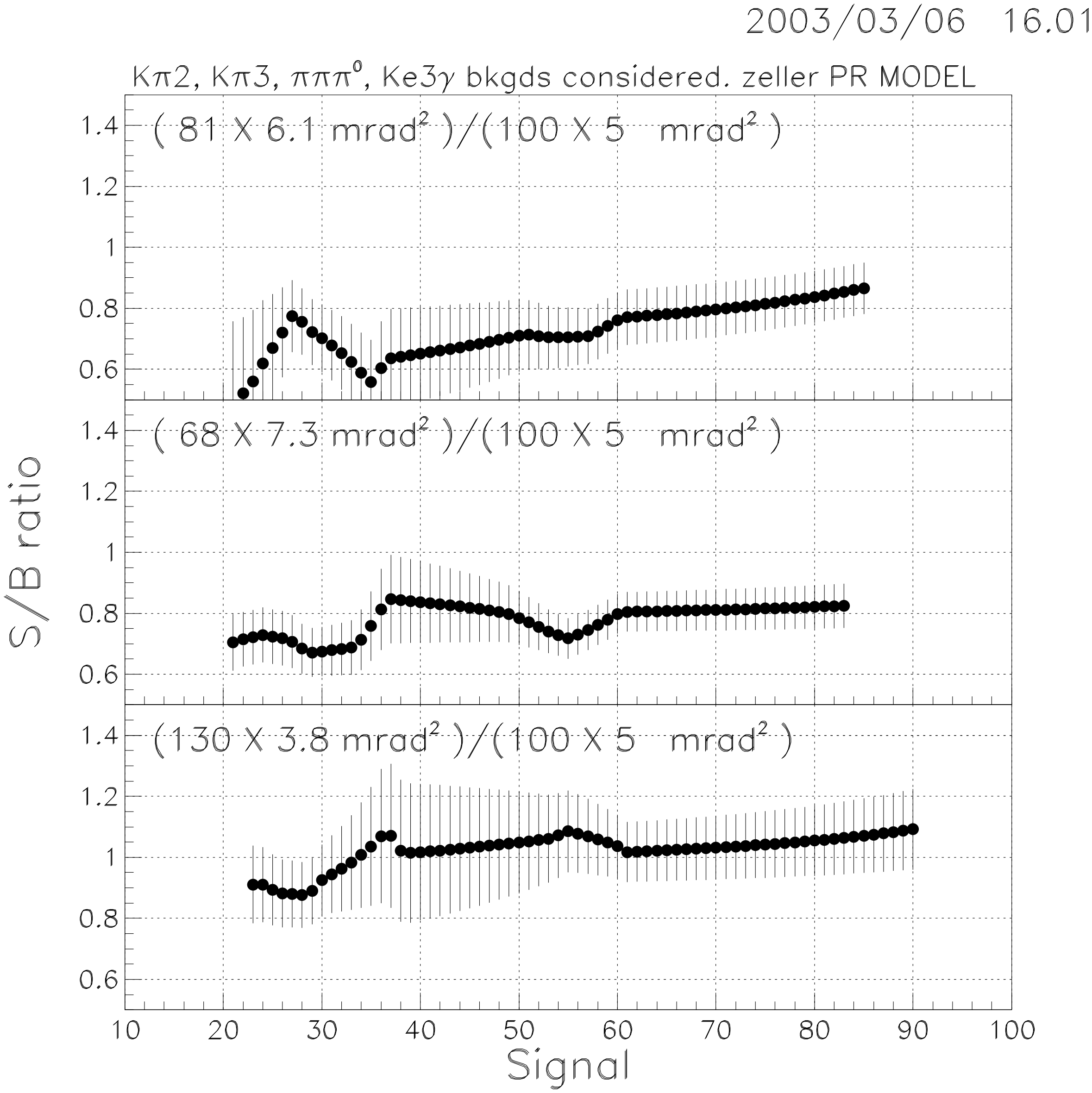

Figure 17: Signal/Background for the three different beam aspect ratios compared to the 100×5 mrad^2 aspect ratio with the Zeller PR model. The uncertainties are statistical only and are correlated from point to point. See text for details.

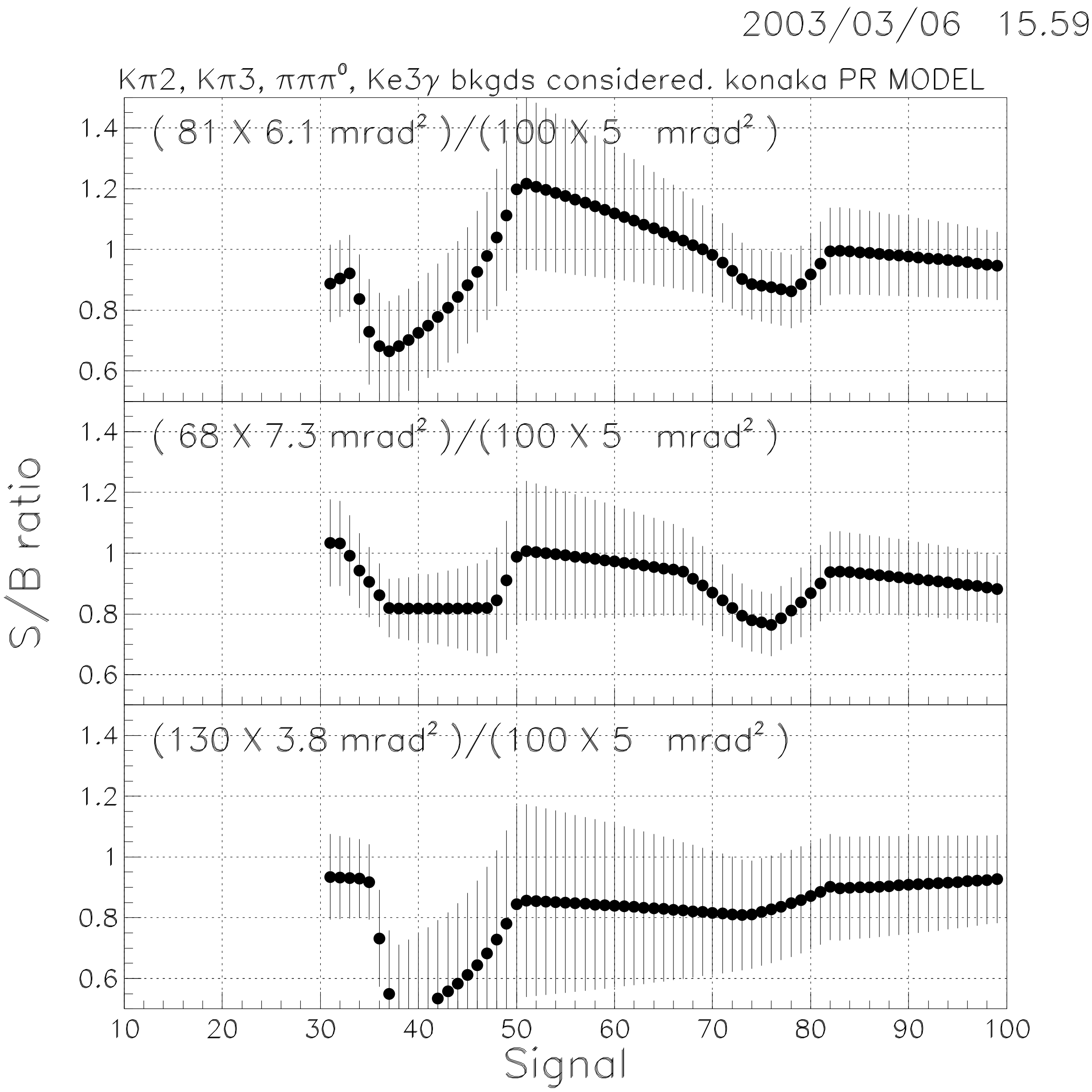

Figure 18: Signal/Background for the three different beam aspect ratios compared to the 100×5 mrad^2 aspect ratio with the Konaka PR model. The uncertainties are statistical only and are correlated from point to point. See text for details.

References

[1] "KOPIO: Measurement of the decay $K_L \rightarrow \pi^\circ \nu \bar{\nu}$, Draft Technical Design Report for the National Science Foundation, TDR, 8 June 2001.

[2] J. Doornbos, "Comparison of the neutron halos for 4 different x-y aspect ratios, for momenta above 750 MeV/c", KOPIO Technical Note TN049, 14 Feb 2003.

[3] D.E. Jaffe, "FastMC estimate of neutron background rates", KOPIO Technical Note TN047, 16 Dec 2002.

[4] P. Kapinos " The estimation of Klong flux at 24 Gev/c", KOPIO Technical Note TN005, 22 Aug 1997.

[5] D. Bryman, "E926 Preradiator Study: Alternating Horizontal and Vertical Anode Wires and Cathode Strips" , KOPIO Technical Note TN014, 25 March 1999.

[6] M. Zeller, "A preradiator for E926 based on a Straw Tube design", KOPIO Technical Note TN006, 2 March 1998.